First Observation and Measurement of the Decay $K^{\pm} \to \pi^{\pm}e^+e^-\gamma$

The NA48/2 Collaboration

J.R. Batley, A.J. Culling, G. Kalmus, C. Lazzeroni, D.J. Munday, M.W. Slater, S.A. Wotton

Cavendish Laboratory, University of Cambridge, Cambridge, CB3 0HE, U.K.[1]

R. Arcidiacono, G. Bocquet, N. Cabibbo, A. Ceccucci, D. Cundy[2], V. Falaleev, M. Fidecaro, L. Gatignon, A. Gonidec, W. Kubischta, A. Norton, A. Maier, M. Patel, A. Peters

CERN, CH-1211 Genève 23, Switzerland

S. Balev, P.L. Frabetti, E. Goudzovski[3], P. Hristov[4], V. Kekelidze, V. Kozhuharov, L. Litov, D. Madigozhin, E. Marinova, N. Molokanova, I. Polenkevich, Yu. Potrebenikov, S. Stoynev, A. Zinchenko

Joint Institute for Nuclear Research, 141980 Dubna, Russian Federation

E. Monnier[5], E. Swallow, R. Winston

The Enrico Fermi Institute, The University of Chicago, Chicago, Illinois, 60126, U.S.A.

P. Rubin, A. Walker

Department of Physics and Astronomy, University of Edinburgh, JCMB King's Buildings, Mayfield Road, Edinburgh, EH9 3JZ, U.K.

W. Baldini, A. Cotta Ramusino, P. Dalpiaz, C. Damiani, M. Fiorini, A. Gianoli, M. Martini, F. Petrucci, M. Savrié, M. Scarpa, H. Wahl

Dipartimento di Fisica dell'Università e Sezione dell'INFN di Ferrara, I-44100 Ferrara, Italy

A. Bizzeti[6], M. Calvetti, E. Celeghini, E. Iacopini, M. Lenti, F. Martelli[7], G. Ruggiero[3], M. Veltri[7]

Dipartimento di Fisica dell'Università e Sezione dell'INFN di Firenze, I-50125 Firenze, Italy

M. Behler, K. Eppard, C. Handel, K. Kleinknecht, P. Marouelli, L. Masetti[8], U. Moosbrugger, C. Morales Morales, B. Renk, M. Wache, R. Wanke, A. Winhart

Institut für Physik, Universität Mainz, D-55099 Mainz, Germany[9]

D. Coward[10], A. Dabrowski, T. Fonseca Martin[4], M. Shieh, M. Szleper, M. Velasco, M.D. Wood[11]

Department of Physics and Astronomy, Northwestern University, Evanston Illinois 60208-3112, U.S.A.

1

G. Anzivino, P. Cenci, E. Imbergamo, A. Nappi, M. Pepe, M.C. Petrucci, M. Piccini,
M. Raggi, M. Valdata-Nappi

Dipartimento di Fisica dell'Università e Sezione dell'INFN di Perugia, I-06100 Perugia, Italy

C. Cerri, G. Collazuol, F. Costantini, L. DiLella, N. Doble, R. Fantechi, L. Fiorini,
S. Giudici, G. Lamanna, I. Mannelli, A. Michetti, G. Pierazzini, M. Sozzi

*Dipartimento di Fisica dell'Università, Scuola Normale Superiore e Sezione dell'INFN di Pisa,
I-56100 Pisa, Italy*

B. Bloch-Devaux, C. Cheshkov [4], J.B. Chèze, M. De Beer, J. Derré, G. Marel,
E. Mazzucato, B. Peyaud, B. Vallage

DSM/DAPNIA - CEA Saclay, F-91191 Gif-sur-Yvette, France

M. Holder, M. Ziolkowski

Fachbereich Physik, Universität Siegen, D-57068 Siegen, Germany [12]

S. Bifani, C. Biino, N. Cartiglia, M. Clemencic [4], S. Goy Lopez, F. Marchetto

*Dipartimento di Fisica Sperimentale dell'Università e Sezione dell'INFN di Torino, I-10125
Torino, Italy*

H. Dibon, M. Jeitler, M. Markytan, I. Mikulec, G. Neuhofer, L. Widhalm

*Österreichische Akademie der Wissenschaften, Institut für Hochenergiephysik, A-10560 Wien,
Austria [13]*

Abstract

Using the full data set of the NA48/2 experiment, the decay $K^{\pm} \to \pi^{\pm} e^+ e^- \gamma$ is observed for the first time, selecting 120 candidates with 7.3±1.7 estimated background events. With $K^{\pm} \to \pi^{\pm} \pi^0_D$ as normalisation channel, the branching ratio is determined in a model-independent way to be $\mathrm{Br}(K^{\pm} \to \pi^{\pm} e^+ e^- \gamma, m_{ee\gamma} > 260\,\mathrm{MeV}/c^2) = (1.19 \pm 0.12_{\mathrm{stat}} \pm 0.04_{\mathrm{syst}}) \times 10^{-8}$. This measured value and the spectrum of the $e^+ e^- \gamma$ invariant mass allow a comparison with predictions of Chiral Perturbation Theory.

Accepted by Phys. Lett. B

1 Introduction

The decay $K^\pm \to \pi^\pm e^+ e^- \gamma$ is similar to the decay $K^\pm \to \pi^\pm \gamma\gamma$, with one of the photons internally converting into a pair of electrons. Both decays can be described in the framework of Chiral Perturbation Theory (ChPT). The lowest order terms are of order p^4, where predominantly loop diagrams contribute to the amplitude [1]. This leads to a characteristic signature in the $e^+ e^- \gamma$ invariant mass distribution, which is favored to be above $2m_{\pi^+}$ and exhibits a cusp at the $2m_{\pi^+}$ threshold. In ChPT, the loop contribution is fixed up to a free parameter $\hat{c}$, which is a function of several strong and weak coupling constants and expected to be of $\mathcal{O}(1)$ [2].

Higher order ChPT calculations on $K^+ \to \pi^+ \gamma\gamma$ have been performed, but are model-dependent. Theoretical predictions for $K^+ \to \pi^+ e^+ e^- \gamma$ exist [3], following the earlier work on $K^+ \to \pi^+ \gamma\gamma$ [2]. The predicted branching ratios lie in the range between 0.9 and 1.7×10^{-8}, for values of $|\hat{c}| \leq 2$. Experimental results are available only for $K^+ \to \pi^+ \gamma\gamma$, based on the observation of 31 signal candidates by the E787 experiment [4].

In this letter, we report the first observation of the decay $K^\pm \to \pi^\pm e^+ e^- \gamma$ and the model-independent measurement of its branching fraction, using $K^\pm \to \pi^\pm \pi_D^0$ with $\pi_D^0 \to e^+ e^- \gamma$ as the normalisation channel. These results have been derived from the full data set of the NA48/2 experiment.

2 Experimental Set-up

The NA48/2 experiment took data in 2003 and 2004 at the CERN SPS. Two beams of charged particles were produced by a 400 GeV/c proton beam impinging on a Be target in a 4.8 s long pulse repeated every 16.8 s. Positive and negative particles with momenta of (60 ± 3) GeV/c were simultaneously selected by an achromatic system, which split the two beams in the vertical plane and then recombined them on a common axis. After passing through a collimator, the beams were split and recombined again in a second achromat. Finally, the two beams passed a cleaning and a defining collimator before entering the decay volume housed in a 114 m long evacuated tank with a diameter between 1.92 and 2.4 m and terminated by a 0.3% radiation lengths thick Kevlar window. The axes of both beams coincided within 1 mm inside the decay volume. The beams were primarily composed of charged pions, with a fraction of $5 - 6\%$ of $K^\pm$. On average, about 4.8×10^5 K^+ and 2.7×10^5 K^- per pulse decayed in the fiducial decay volume. A more detailed description of the beamline can be found in [5].

The decay region was followed by the NA48 detector [6]. The momenta and positions of charged particles were measured in a magnetic spectrometer. The spectrometer was housed in a helium gas volume and consisted of two pairs of drift chambers before and after a dipole magnet with vertical magnetic field direction, giving a horizontal transverse momentum kick of 120 MeV/c. Each chamber had four views (x, y, u, v) with two sense wire planes in each view. The u and v views were inclined by $\pm 45°$ with respect to the x-y plane. The space points, reconstructed by each chamber, had a resolution of 150 μm in each projection. The momentum resolution of the spectrometer in 2003/2004 was measured to

be $\sigma_p/p = 1.02\% \oplus 0.044\% \times p$, with p in GeV/c. The magnetic spectrometer was followed by a segmented plastic scintillator hodoscope with one plane of vertical and one plane of horizontal strips, respectively. It was used to produce fast trigger signals and to provide precise time measurements of charged particles. The time resolution of the hodoscope was better than 200 ps.

Photon and electron energies were measured with a 27 radiation length thick liquid-krypton electromagnetic calorimeter (LKr). It was read out longitudinally in 13248 cells of 2×2 cm^2 cross-section. The energy resolution was determined to be $\sigma_E/E = 3.2\%/\sqrt{E} \oplus 9\%/E \oplus 0.42\%$, with E in GeV. The spatial and time resolutions were better than 1.3 mm and 300 ps, respectively, for photon and electron clusters above 20 GeV.

Additional detector elements, such as the hadron calorimeter and the muon and photon veto counters, were not used in the present analysis.

The events were selected by a two-level trigger which was optimised for events with three charged tracks. At the first level, three-track events were triggered by requiring coincidences of hits in the two hodoscope planes. The second level trigger was based on the hit coordinates in the drift chambers. It required at least two tracks to originate from the decay volume with a reconstructed distance of closest approach of less than 5 cm. The trigger efficiency for the selection of the normalisation channel $K^\pm \to \pi^\pm \pi_D^0$ was $(96.48 \pm 0.05)\%$, determined from data events taken with a down-scaled complementary trigger.

In total, NA48/2 collected about 18×10^9 triggers. In the course of data-taking, the magnet polarities of both the beamline and the spectrometer were regularly reversed to have similar conditions for decays of positive and negative kaons.

3 Monte Carlo Simulation

In order to compute the acceptance of signal, normalisation, and background channels, a detailed GEANT-based [7] Monte Carlo simulation was employed, which included the full detector and material description, stray magnetic fields, drift chamber inefficiencies and misalignment, and beamline simulation.

For the signal channel, the full matrix element was used [3], with a value of $\hat{c} = 1.8$, in agreement with the measurement of $K^+ \to \pi^+ \gamma\gamma$ [4].

For all other channels, if not otherwise mentioned below, the known theoretical matrix elements were used. Radiative corrections were applied to the simulation of signal, normalisation, and $K^\pm \to \pi^\pm e^+ e^-$ by using the PHOTOS package [8].

4 Data Selection

The analysis described here is based on the full data set of the NA48/2 experiment, recorded in 2003 and 2004. The selection of the signal events was performed in two steps. At first, described in the next section, a set of basic selection criteria was applied to define the signal region and to assure the quality of the selected candidate events. In a second step, described

in the following section, further selection criteria were applied to suppress contributions of the various background sources.

4.1 Event Selection

Each selected event had to have at least one combination of three tracks with a total charge of ± 1 and one cluster in the LKr calorimeter not associated with any track. Each track was required to have a radial distance from the detector axis of at least 12 cm in the first drift chamber and to lie well inside the active LKr calorimeter region, i.e. well inside its outer edge and more than 15 cm from the detector axis. The distance between any two tracks in the first drift chamber had to exceed 2 cm. This latter requirement rejects all events with external photon conversions in the detector material before the spectrometer.

The three tracks had to be compatible with originating from the same decay vertex and to have a distance of closest approach of less than 4 cm for each of the three pairs of two tracks. The longitudinal position of the reconstructed decay vertex had to be more than 2 m and less than 98 m down-stream of the final collimator and within a radius of 3 cm around the beam axis. The track times, measured in the scintillator hodoscope, had to be at most ± 3 ns from the mean of the track times. In less than 1% of the events, no hodoscope information was available for at least one track. For those events, the track times measured in the drift chambers were taken and required to be at most ± 6 ns from the mean track time.

Pions and electrons were identified by the ratio E/p of energy deposited in the LKr calorimeter and momentum measured in the spectrometer. Electrons and pions were required to have $E/p > 0.94$ and $E/p < 0.8$, respectively. With these requirements the probability for mis-identification of electrons or pions is of the order of a few per mille. Two tracks of opposite charge had to be identified as electrons with each having a momentum greater than 3 GeV/c. The third track had to be a pion candidate and had to have a momentum greater than 4 GeV/c.

Photon candidates were defined as calorimeter clusters unassociated to charged tracks and required to lie 15 cm from the detector axis and well inside the outer edge of the LKr. The distance to the projected impact point of any pion candidate had to exceed 25 cm, the distance to the electron tracks or any other possible cluster had to exceed 10 cm. The reconstructed cluster energy had to be greater than 3 GeV, and the time difference to the mean of the cluster time and the track times measured in the drift chambers had to be smaller than 6 ns.

The sum of pion, electron, positron, and photon momenta was required to be between 54 and 66 GeV/c. An energy centre-of-gravity $(x_{\text{cog}}, y_{\text{cog}}) = (\sum_i x_i E_i / \sum_i E_i, \sum_i y_i E_i / \sum_i E_i)$ was defined by using the transverse positions x_i and y_i and the energies E_i of the projected tracks and the photon cluster at the front surface of the LKr calorimeter. The tracks were projected onto the LKr surface from their positions and directions in the first drift chamber before the spectrometer magnet. The radial distance between the energy centre-of-gravity and the beam had to be less than 3 cm.

To suppress background events coming from decays with more than one photon, we required that no other unassociated cluster was in-time with the event. Since this would reject

5

also events with photons from bremsstrahlung on detector material or with shower fluctuations of pion showers, we still allowed additional clusters with $E\,[\mathrm{GeV}] < 7 - 0.14\,d_e\,[\mathrm{cm}]$ or $E\,[\mathrm{GeV}] < 15 - 0.25\,d_\pi\,[\mathrm{cm}]$, where d_e and d_π are the distances of the cluster to the impact point of an electron and the pion track, respectively. This requirement against additional unassociated clusters rejected about 0.3% of all events.

With these basic selection criteria, a sample of about 22.8 million events was obtained. At this level of the selection, the data were dominated by $K^\pm \to \pi^\pm \pi_D^0$ decays, where the π^0 underwent a Dalitz decay $\pi_D^0 \to e^+ e^- \gamma$.

4.2 Background Suppression

A number of additional selection criteria had to be applied to effectively suppress the remaining background. In the following, we examine the possible sources of background to the signal.

- **$K^\pm \to \pi^\pm \pi_D^0$, $K^\pm \to \pi_D^0 e^\pm \nu$, and $K^\pm \to \pi_D^0 \mu^\pm \nu$ decays**

  The decay $K^\pm \to \pi^\pm \pi_D^0$ ($K_{2\pi D}$) with $\pi_D^0 \to e^+ e^- \gamma$ has exactly the same signature as the signal channel. We therefore rejected events for which $120\ \mathrm{MeV}/c^2 < m_{e^+ e^- \gamma} < 150\ \mathrm{MeV}/c^2$. To evaluate this requirement, we assigned the electron mass to each track and applied the cut to both opposite-charged track combinations. This completely rejects also the semileptonic decays $K^\pm \to \pi_D^0 e^\pm \nu$ and $K^\pm \to \pi_D^0 \mu^\pm \nu$ as well as the small amount of doubly-misidentified $K_{2\pi D}$ events, where both the pion and an electron are misidentified.

- **$K^\pm \to \pi^\pm \pi_D^0 \gamma$ decays**

  The decay $K^\pm \to \pi^\pm \pi_D^0 \gamma$ consists of two amplitudes: Inner Bremsstrahlung (IB) and Direct Emission (DE). If the radiative photon is lost, the decay is rejected by the cut against $K^\pm \to \pi^\pm \pi_D^0$ decays. However, if the photon of the π_D^0 decay is lost, the decay may fake a signal event. $K^\pm \to \pi^\pm \pi_D^0 \gamma$ events are the major background source and contribute with 3.1 ± 0.5 IB and 0.12 ± 0.03 DE events, as determined from the simulation, using the measured rates of IB and DE transitions [9].

- **$K^\pm \to \pi^\pm \pi^0 e^+ e^-$ decays**

  The decay $K^\pm \to \pi^\pm \pi^0 e^+ e^-$, which comes from $K^\pm \to \pi^\pm \pi^0 \gamma$ with an internal conversion of the additional photon, has not been measured yet. By evaluating the internal conversion probability, we estimated its branching fraction to be half of that of $K^\pm \to \pi^\pm \pi_D^0 \gamma$. Due to the uncertainty of the estimation, we assigned a $\pm 50\%$ systematic uncertainty to this value. $K^\pm \to \pi^\pm \pi^0 e^+ e^-$ events were simulated by modifying the $K^\pm \to \pi^\pm \pi^0 \gamma$ simulation; the conversion of the photon was added by generating the photon mass with a probability density proportional to the inverse square of the photon mass. The ratio of IB and DE amplitudes was taken from $K^\pm \to \pi^\pm \pi^0 \gamma$ decays [9]. From this, we estimated the amount of background from $K^\pm \to \pi^\pm \pi^0 e^+ e^-$ to $1.6 \pm 0.5 \pm 0.7$ events, where the second uncertainty comes from the estimation of the branching fraction. The contribution from DE is practically negligible.
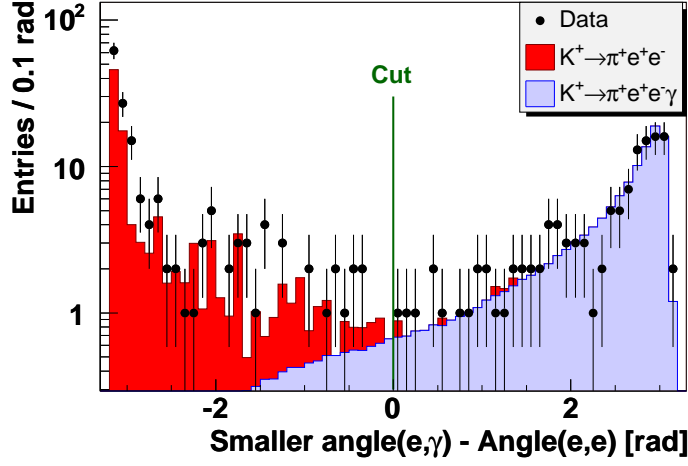
Figure 1: Difference of the smaller of the angles between the photon and $e^{\pm}$ and the angle between e^+ and e^- in the $e^+e^-\gamma$ rest frame for data (circles) and signal and radiative $K^{\pm} \to \pi^{\pm}e^+e^-$ MC simulation.

- **Radiative $K^{\pm} \to \pi^{\pm}e^+e^-$ decays**

  The probability of the rare decay $K^{\pm} \to \pi^{\pm}e^+e^-$ with an observable γ from internal or external bremsstrahlung is of $\mathcal{O}(10^{-8})$, similar to the signal channel. To reject these events, we made use of the different decay kinematics in the $e^+e^-\gamma$ rest frame. For the signal, the photon repels from the e^+e^- system, while in case of $K^{\pm} \to \pi^{\pm}e^+e^- + \gamma_{\mathrm{brems}}$ the electrons, in the $e^+e^-\gamma$ rest frame, fly back-to-back, and the photon is close to one of them. We therefore required $\sphericalangle(e^+, e^-) < \min(\sphericalangle(e^{\pm}, \gamma))$ for the angles between e^+ and e^- and between $e^{\pm}$ and the photon, respectively, in the $e^+e^-\gamma$ rest frame (see Figure 1). The remaining background from $K^{\pm} \to \pi^{\pm}e^+e^-$ decays was determined to be 0.8 ± 0.5 events from MC simulation. This estimate includes a systematic error of $\pm 50\%$, which reflects a disagreement between $K^{\pm} \to \pi^{\pm}e^+e^-$ data and MC in event numbers in the region with $\sphericalangle(e^+, e^-) > \min(\sphericalangle(e^{\pm}, \gamma))$.

- **$K^{\pm} \to \pi^{\pm}\pi^0\pi^0_D$ decays**

  The decay $K^{\pm} \to \pi^{\pm}\pi^0\pi^0_D$ was strongly suppressed by the cut on additional clusters and the rejection of the π^0_D decays. Its contribution to the signal region was estimated by MC simulation to be 0.7 ± 0.7 events.

- **Accidental activity**

  Accidental overlap of separate events may fake signal events. To estimate the amount of such events in the signal sample, we studied the sidebands of the time distributions

in the hodoscope and the LKr calorimeter. One event was found in the calorimeter time sideband, which corresponds to a background estimation of 1 ± 1 events from accidental activity.

Other potential sources of background as e.g. $K^{\pm} \to \pi^{\pm}\pi^{+}\pi^{-}(\gamma)$, $K^{\pm} \to \pi^{+}\pi^{-}e^{\pm}\nu(\bar{\nu})$, or $K^{\pm} \to \pi^{0}\pi_D^{0}e^{\pm}\nu(\bar{\nu})$ were found to be irrelevant.

The signal region was defined by requiring $480 < m_{\pi^{\pm}e^{+}e^{-}\gamma} < 505$ MeV/c^2. Since ChPT predicts only small signal rate and the background increases for low values of $m_{e^{+}e^{-}\gamma}$, we also required $m_{e^{+}e^{-}\gamma} > 260$ MeV/c^2. 120 signal candidates were found, including an estimated total background of 7.3 ± 1.7 events. The background channels are listed in Table 1 together with their respective branching fractions and expected contributions to the signal. All background expectations were obtained by normalising to the total kaon flux.

The signal acceptance, as determined from MC simulation, depends on $m_{e^{+}e^{-}\gamma}$. It was between 6% and 7% for $260 < m_{e^{+}e^{-}\gamma} < 330$ MeV/c^2, and decreased to 2.5% for events near the kinematical edge. The projections of the signal candidates on $m_{\pi^{\pm}e^{+}e^{-}\gamma}$ and $m_{e^{+}e^{-}\gamma}$, together with the background contributions, are shown in Figure 2.

Background source	Branching ratio	Expected events
$K^{\pm} \to \pi^{\pm}\pi_D^{0}\gamma$ (IB)	3.3×10^{-6}	3.1 ± 0.5
$K^{\pm} \to \pi^{\pm}\pi_D^{0}\gamma$ (DE)	5.3×10^{-8}	0.12 ± 0.03
$K^{\pm} \to \pi^{\pm}\pi^{0}e^{+}e^{-}$ (IB)	$\sim 1.7 \times 10^{-6}$	1.6 ± 0.9
$K^{\pm} \to \pi^{\pm}\pi^{0}e^{+}e^{-}$ (DE)	$\sim 2.6 \times 10^{-8}$	0.02 ± 0.01
$K^{\pm} \to \pi^{\pm}e^{+}e^{-}$	2.9×10^{-7}	0.8 ± 0.5
$K^{\pm} \to \pi^{\pm}\pi^{0}\pi_D^{0}$	2.1×10^{-4}	0.7 ± 0.7
Accidentals	—	1.0 ± 1.0
Sum		7.3 ± 1.7

Table 1: Relevant background sources and number of expected events in the signal region with all selection criteria applied. Except for $K^{\pm} \to \pi^{\pm}\pi^{0}e^{+}e^{-}$, the branching fractions are taken from [9]; for $K^{\pm} \to \pi^{\pm}\pi_D^{0}\gamma$ and $K^{\pm} \to \pi^{\pm}\pi^{0}e^{+}e^{-}$ they are defined for $T_{\pi} = 55 - 90$ MeV.

4.3 Normalisation Channel

For the normalisation channel $K^{\pm} \to \pi^{\pm}\pi_D^{0}$ exactly the same selection as for the signal was applied, but without the criteria on the $e^{+}e^{-}\gamma$ invariant mass and the $e^{+}e^{-}\gamma$ decay angles. Instead, the $e^{+}e^{-}\gamma$ invariant mass was required to be within $m_{\pi^0} - 35$ MeV/c^2 and $m_{\pi^0} + 30$ MeV/c^2. The asymmetry of this cut takes into account the radiative tail in the $m_{e^{+}e^{-}\gamma}$ distribution. We found about 18.7 million $K_{2\pi D}$ candidates including an estimated background of about 0.5%. The acceptance of the selection was determined to be 5.0% from MC simulation. The branching fraction of the normalisation is Br($K^{\pm} \to \pi^{\pm}\pi_D^{0}, \pi_D^{0} \to e^{+}e^{-}\gamma) = (2.51 \pm 0.07) \times 10^{-3}$ [9]. From this, we determined the total flux of kaon decays in the fiducial volume to be $\Phi_K = (1.48 \pm 0.04) \times 10^{11}$.
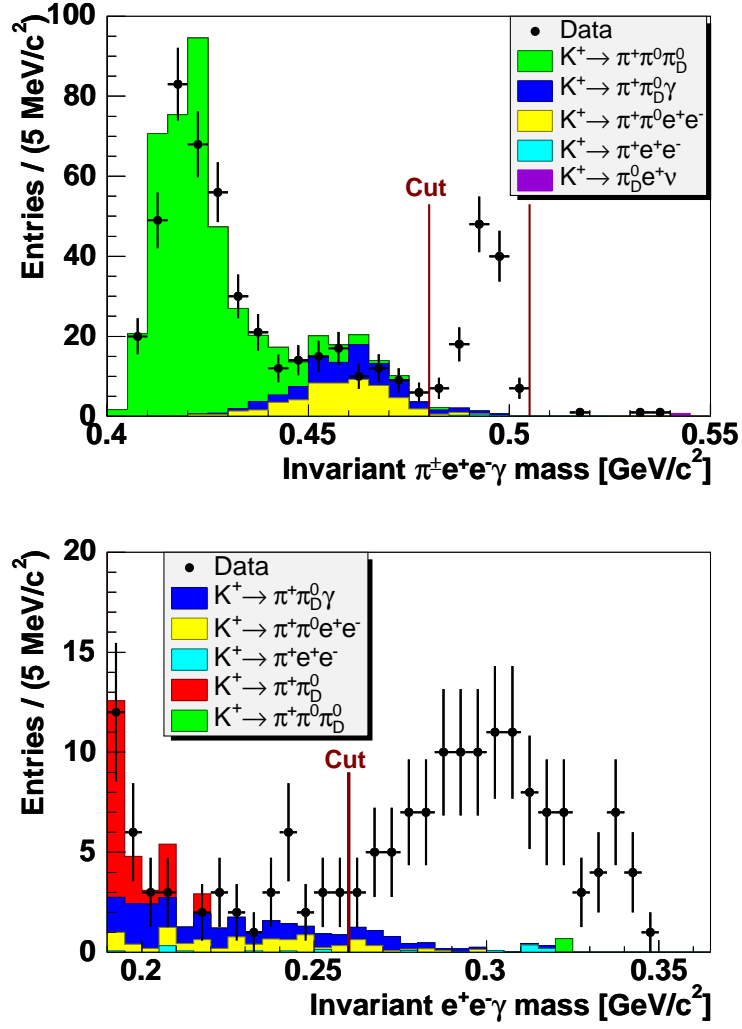
Figure 2: Selected signal candidates and background expectation from MC simulation: (top) $\pi^\pm e^+ e^- \gamma$ invariant mass, (bottom) $e^+ e^- \gamma$ invariant mass. The vertical lines indicate the accepted region for the branching ratio measurement.

5 Results

To determine the branching fraction in a model-independent way, we computed a partial branching fraction for each 5 MeV/c^2 wide $m_{e^+e^-\gamma}$ interval i from

$$\mathrm{Br}_i(K^\pm \to \pi^\pm e^+ e^- \gamma) \,=\, \frac{N_i^{\pi ee\gamma} - N_i^{\mathrm{bkg}}}{A_i^{\pi ee\gamma} \cdot \epsilon} \times \frac{1}{\Phi_K},$$

with the numbers $N_i^{\pi ee\gamma}$ and N_i^{bkg} of observed signal and estimated backgrounds events, and the signal acceptance $A_i^{\pi ee\gamma}$ in bin i. The overall trigger efficiency is ϵ and Φ_K the total kaon flux. By summing over the bins above $m_{e^+e^-\gamma} = 260$ MeV/c^2, we obtained $\mathrm{Br}(K^\pm \to \pi^\pm e^+ e^- \gamma, m_{e^+e^-\gamma} > 260$ MeV/$c^2) = (1.19 \pm 0.12_{\mathrm{stat}}) \times 10^{-8}$, where the error is from data statistics only. This result is independent of the value of $\hat{c}$ and any theoretical assumption of the $m_{e^+e^-\gamma}$ distribution.

Several potential sources of systematic errors can affect the result and have been studied.

The background estimation has a total uncertainty of ± 1.7 events, as explained before, which results in an uncertainty of $\pm 1.5\%$ on the result.

Possible imperfections of the description of the detector acceptance in the Monte Carlo simulation might also cause systematic effects on the branching fraction measurement. For an estimation of such effects we have varied the main selection cuts. To not fall victim of statistical fluctuations in the signal channel, the variations have only been performed in the normalization channel. This leads to a conservative estimate, since detector systematics are expected to cancel between signal and normalization. We found maximum changes of the result of the order of $\pm 0.4\%$, which we assigned as the systematic uncertainty due to the detector acceptance.

The particle identification via the E/p ratio could not be perfectly modelled in the simulation. However, the inefficiencies are expected to almost completely cancel between signal and normalization mode. The residual uncertainty on the electron identification was measured from K_{e3}^0 decays to better than 0.1%. The uncertainty of the pion identification efficiency was determined from variations of the E/p criterion in the normalization channel to be at most $\pm 0.3\%$. Combining both, we assigned a total uncertainty of $\pm 0.4\%$ due to particle identification.

The overall trigger efficiency should be the same for signal and normalisation to a great extent. A difference could only arise from the slightly different event topologies. Due to the lack of statistics, the trigger efficiency could not be measured for signal events. We therefore studied the dependency of the trigger efficiency of $K^\pm \to \pi^\pm \pi_D^0$ events as a function of the event topology. From this, we obtained a systematic uncertainty of $\pm 0.6\%$.

The statistical error of the signal and normalisation MC samples contributes to $\pm 0.9\%$.

Finally, the external inputs of $\mathrm{Br}(K^\pm \to \pi^\pm \pi_D^0)$ and $\mathrm{Br}(\pi_D^0 \to e^+ e^- \gamma)$ add an uncertainty of $\pm 2.7\%$ [9]. This is identical with the error quoted on the kaon flux in Section 4.3.

All uncertainties of the measurement are listed in Table 2. The final result on the branching ratio is

$$\mathrm{Br}(K^\pm \to \pi^\pm e^+ e^- \gamma, m_{e^+e^-\gamma} > 260\,\mathrm{MeV}/c^2) \,=\, (1.19 \pm 0.12_{\mathrm{stat}} \pm 0.04_{\mathrm{syst}}) \times 10^{-8}.$$

Source	ΔBr/Br	ΔBr $[10^{-8}]$
Background subtraction	$\pm 1.5\%$	± 0.017
Electron/pion identification	$\pm 0.4\%$	± 0.005
Detector acceptance	$\pm 0.4\%$	± 0.005
Trigger efficiency	$\pm 0.6\%$	± 0.007
MC statistics	$\pm 0.9\%$	± 0.011
Normalisation	$\pm 2.7\%$	± 0.032
Total systematic uncertainty	$\pm 3.3\%$	± 0.04
Statistical uncertainty	$\pm 9.7\%$	± 0.12

Table 2: Summary of uncertainties of the branching ratio measurement.

The distribution of the partial branching fractions is shown in Figure 3 and tabulated in Table 3. The quoted errors are confidence intervals for the unknown true value. We chose Pearson's χ^2 intervals for Poisson statistics [10] for them, defined as $\sigma_{\pm} = \sqrt{n_i + 1/4} \pm 1/2$ for each data bin with entry n_i, before background subtraction, acceptance correction, and normalisation. The uncertainties on the background and acceptance estimates were added in quadrature in each bin, while the global systematic uncertainties — dominated by the normalisation — are not quoted in Figure 3 and Table 3.

We used the measured branching fraction and the shape of the $e^+e^-\gamma$ spectrum to extract a value for the parameter $\hat{c}$. Performing a least squares fit of the absolute prediction given in ref. [3] to the data with $m_{e^+e^-\gamma} > 260$ MeV/c^2, we obtained $\hat{c} = 0.90 \pm 0.45$, where the error is dominated by the data statistics. The quality of the fit was $\chi^2/n_{\mathrm{dof}} = 8.1/17$. This result is in agreement within about 1.2 standard deviations with the value of 1.8 ± 0.6, previously measured in $K^+ \to \pi^+\gamma\gamma$ [4], and has a somewhat smaller error. Figure 3 shows the predicted spectrum for our best fit value of $\hat{c}$ and the previously found value, together with the background and acceptance corrected data.

Using our measured value of $\hat{c}$ and ref. [3], we computed the differential branching fraction for $m_{e^+e^-\gamma} < 260$ MeV/c^2 and added it to our measured result. We then obtained for the total branching fraction Br($K^{\pm} \to \pi^{\pm}e^+e^-\gamma$) $= (1.29 \pm 0.13_{\mathrm{exp}} \pm 0.03_{\hat{c}}) \times 10^{-8}$, where the first uncertainty is the combined statistical and systematic error, and the second reflects the uncertainty in $\hat{c}$.
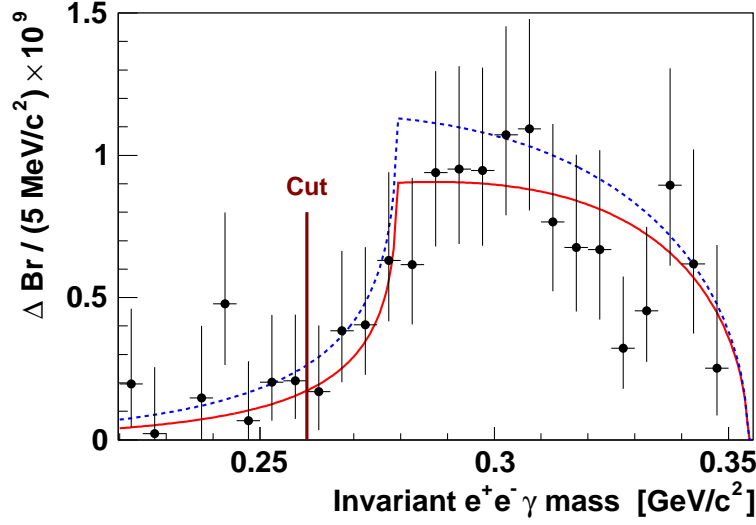
6 Acknowledgements

Figure 3: Partial $K^{\pm} \to \pi^{\pm} e^{+} e^{-} \gamma$ branching fractions as function of the $e^{+} e^{-} \gamma$ invariant mass. The signal region is defined for $m_{e^{+}e^{-}\gamma} > 260$ MeV/c^2. The lines are the expectations from ref. [3] for $\hat{c} = 0.90$ (solid, best fit) and $\hat{c} = 1.8$ (dashed, estimate from $K^{+} \to \pi^{+} \gamma\gamma$ [4]).

$m_{e^{+}e^{-}\gamma}$ interval	Δ Br $[10^{-9}]$	$m_{e^{+}e^{-}\gamma}$ interval	Δ Br $[10^{-9}]$
$260 - 265$ MeV/c^2	$0.17 \, ^{+0.23}_{-0.13}$	$305 - 310$ MeV/c^2	$1.09 \, ^{+0.39}_{-0.29}$
$265 - 270$ MeV/c^2	$0.38 \, ^{+0.28}_{-0.18}$	$310 - 315$ MeV/c^2	$0.77 \, ^{+0.34}_{-0.24}$
$270 - 275$ MeV/c^2	$0.40 \, ^{+0.27}_{-0.18}$	$315 - 320$ MeV/c^2	$0.68 \, ^{+0.33}_{-0.23}$
$275 - 285$ MeV/c^2	$0.63 \, ^{+0.31}_{-0.21}$	$320 - 325$ MeV/c^2	$0.67 \, ^{+0.35}_{-0.25}$
$280 - 280$ MeV/c^2	$0.62 \, ^{+0.30}_{-0.21}$	$325 - 330$ MeV/c^2	$0.32 \, ^{+0.25}_{-0.14}$
$285 - 295$ MeV/c^2	$0.94 \, ^{+0.36}_{-0.26}$	$330 - 335$ MeV/c^2	$0.45 \, ^{+0.29}_{-0.18}$
$290 - 290$ MeV/c^2	$0.95 \, ^{+0.36}_{-0.26}$	$335 - 340$ MeV/c^2	$0.89 \, ^{+0.41}_{-0.28}$
$295 - 300$ MeV/c^2	$0.95 \, ^{+0.36}_{-0.26}$	$340 - 345$ MeV/c^2	$0.62 \, ^{+0.40}_{-0.25}$
$300 - 305$ MeV/c^2	$1.07 \, ^{+0.38}_{-0.28}$	$345 - 350$ MeV/c^2	$0.25 \, ^{+0.43}_{-0.17}$

Table 3: Partial $K^{\pm} \to \pi^{\pm} e^{+} e^{-} \gamma$ branching fractions dependent on the $e^{+} e^{-} \gamma$ invariant mass. Quoted are uncertainties from data and MC statistics and background estimation. All other uncertainties are completely correlated and amount to $\pm 3.2\%$, dominated by the normalisation.

References

[1] G. Ecker, A. Pich, and E. de Rafael, *Nucl. Phys.* B **303** (1988), 665.

[2] G. D'Ambrosio and J. Portolés, *Phys. Lett.* B **386** (1996), 403.

[3] F. Gabbiani, *Phys. Rev.* D **59** (1999), 094022.

[4] P. Kitching *et al.* (E787 Collaboration), *Phys. Rev. Lett.* **79** (1997), 4079.

[5] J.R. Batley *et al.* (NA48/2 Collaboration), CERN-PH-EP-2007-021 (arXiv:0707.0697), submitted to *Eur. Phys. J.* C.

[6] V. Fanti *et al.* (NA48 Collaboration), *Nucl. Instrum. Methods* A **574** (2007), 433.

[7] GEANT Detector Description and Simulation Tool, CERN Program Library Long Write-up W5013 (1994).

[8] E. Barberio and Z. Was, Comp. Phys. Comm. **79** (1994), 291.

[9] W.M. Yao *et al.* (Particle Data Group), J. Phys. **G 33** (2006), 1.

[10] G. Cowan, "Statistical Data Analysis", Oxford University Press, Oxford, 1998.